P452 Term Paper Report
An investigation of the role of enhanced permeability for aseismic slip triggered by subsurface fluid injection

Ratul Das[1, *]

[1] *School of Physical Sciences, National Institute of Science Education and Research, HBNI, Jatni, Khordha, Odisha-752050, India*

(Dated: April 24, 2024)

Induced seismicity due to subsurface fluid injection is a problem of interest in geology, civil engineering, and mechanical engineering due to the industrial relevance of such injection. Due to the nonlinear nature of how materials respond to stress when fluids are involved, a number of problems remain insufficiently addressed in the literature. In this term paper project, I explored how slip occurs in a crack due to the evolution of pore pressure across it as a result of fluid injection in the case when permeability enhancement is taken into account. I made use of a backward differentiation formula (BDF) method to solve for the pore pressure at the crack, and then obtained the slip across the crack using the boundary element method (BEM), which is a type of finite element method (FEM). Through this formulation in Python, I compared results in cases of various parameters in order to examine the circumstances under which the the aseismic slip front outruns the pore pressure front, causing quicker-than-expected seismicity around fluid injection sites.

I. INTRODUCTION

Large fluid volume injection in the subsurface is increasingly common across a range of economic (enhanced oil recovery, geothermal energy extraction) and remediation (CO2 sequestration, wastewater injection) activities. However, deep fluid injections into the subsurface are often associated with increased seismicity within a few hundreds of kilometres of the injection site, with earthquakes as large as M∼6.0 being recorded in some situations (Keranen et al., 2014). Such injection-induced seismicity is usually ascribed to reduction in fault strength on pre-stressed faults due to diffusive pore-pressure increase in the surrounding subsurface volume. However, based on recent in-situ experiments and theoretical work, it has been suggested that fluid-injection might primarily induce aseismic fault slip instead. This observed seismicity is then driven by elastic stress-perturbations induced by the propagation of the aseismic slip front. If such an aseismic rupture can outpace pore pressure diffusion as recently suggested by in-situ experiments, then injection-induced seismicity can also occur outside the pore pressurized region.

II. WORKING PRINCIPLE

The method that is described in Fehlberg's 1969 paper ([2]) is novel due to the reason that it is an 'embedded' method from the RK family of methods. In embedded methods, identical function evaluations are used together to create methods of multiple orders and similar error constants. Fehlberg's algorithm (also known as the RKF45 method) is a 4th order method, but it has a 5th order error estimator. With the performance of an extra calculation, the solution's error can be estimated and regulated accordingly by using the higher-order embedded method that allows for a step size to be determined dynamically.

III. METHODOLOGY

We model the rupture as a 1D single mode anti-plane strain crack, coupled with a pore pressure perturbation profile with and without poro-elastic enhancement of permeability. Our model consists of the following three parts:

- Mode III crack based integral equation relating shear stress on the fault plane to the slip gradient by the equation of quasi-static elastic equilibrium (Bilby and Eshelby, 1968).
- Slip weakening friction.
- Pore pressure perturbation: both constant permeability and enhanced permeability.

A. Rupture model

The rupture model used is based on the representation of a shear crack as a linear superposition of screw dislocations (Bilby and Eshelby, 1968). It is derived from the consituitive Hooke's law and it relates shear stress on the fault plane to the slip gradient. For a plane away from a free surface (like a fault plane), the equation is as follows(After Viesca and Rice, 2012)

* ratul.das@niser.ac.in

The higher order step is computed as,

$$\tau(x,t) = \tau_b - \frac{\mu^*}{2\pi}\int_{a_-}^{a_+}\frac{\partial\delta(s,t)}{\partial s}\frac{ds}{x-s} \tag{1}$$

$$\int_{-1}^{1}\frac{F(y)}{\sqrt{1-y^2}}dy = \frac{\pi}{n}\sum_{j=1}^{n}F\left(y_j\right) \tag{2}$$

$$f\left(\sigma_0 - \Delta p(x,t)\right) = \tau_b - \frac{\mu^*}{2\pi}\int_{a_-}^{a_+}\frac{\partial\delta(s,t)}{\partial s}\frac{ds}{x-s} \tag{3}$$

B. Friction law

$$\begin{aligned} f(\delta(s,t)) &= f_p - w\delta(s,t) \\ f(\delta(s,t)) &= f_p - \frac{f_p - f_r}{\delta_r}\delta(s,t) \end{aligned} \tag{4}$$

C. Pore pressure profile

1. Point-source constant pressure case

$$\frac{\partial p(x,t)}{\partial t} = \alpha\frac{\partial^2 p(x,t)}{\partial x^2} \tag{5}$$

$$p(x,t) = p_0 + \Delta p\Pi(\xi)$$

2. Enhanced Permeability solution

$$k = k_0 e^{\gamma p} \implies \alpha = \alpha_o e^{\gamma p} \tag{6}$$

$$\frac{\mu}{S_s}\frac{\partial p(x,t)}{\partial t} = \frac{\partial}{\partial x}\left(k\frac{\partial p(x,t)}{\partial x}\right) \tag{7}$$

$$\begin{aligned} &\implies \frac{\partial p(x,t)}{\partial t} = \frac{\partial}{\partial x}\left(\alpha(p)\frac{\partial p(x,t)}{\partial x}\right) \\ &\implies \frac{\partial p(x,t)}{\partial t} = \frac{\partial}{\partial x}\left(\alpha_0 e^{\gamma p}\frac{\partial p(x,t)}{\partial x}\right) \\ &\implies \frac{\partial p(x,t)}{\partial t} = \alpha_0 e^{\gamma p}\gamma\left(\frac{\partial p}{\partial x}\right)^2 + \alpha_0 e^{\gamma p}\frac{\partial^2 p}{\partial x^2} \end{aligned} \tag{8}$$

$$p = \frac{1}{\gamma}\ln(\gamma\eta) \implies \eta = \frac{1}{\gamma}\exp(\gamma p) \tag{9}$$

$$\frac{\partial\eta}{\partial t} = \alpha_o\gamma\eta\frac{\partial^2\eta}{\partial x^2} \tag{10}$$

$$(\frac{\partial\eta}{\partial t})_i = \alpha_o\gamma\eta(i)\frac{\eta(i+1) - 2\eta(i) + \eta(i-1)}{\Delta x^2} \tag{11}$$

D. Numerical approximations and model setup

1. Rupture model for point-source constant pressure case

$$\tau_s(x,t) = f(\sigma_0 - \Delta p(x,t)) \tag{12}$$

$$\text{where } \Delta p(x,t) = \Delta p_{max} erfc\left(\left|\frac{x}{(\alpha t)^{1/2}}\right|\right)$$

$$\tau_s(x,t) = \tau_b - \frac{\mu^*}{2\pi}\int_{a_-}^{a_+}\frac{\partial\delta(s,t)}{\partial s}\frac{ds}{x-s} \tag{13}$$

$$f(\sigma_0 - \Delta p(x,t)) = \tau_b - \frac{\mu^*}{2\pi}\int_{a_-}^{a_+}\frac{\partial\delta(s,t)}{\partial s}\frac{ds}{x-s} \tag{14}$$

$$(1-\frac{\tau_b}{f\sigma_0}) - \frac{\Delta p_{max} erfc(|\ \lambda\overline{x}\ |)}{\sigma_o} = -\frac{1}{2\pi}\int_{-1}^{+1}\frac{\partial\overline{\delta}(\overline{s},t)}{\partial\overline{s}}\frac{d\overline{s}}{\overline{x}-\overline{s}} \tag{15}$$

$$\begin{aligned} I(x_i) &= \int_{-1}^{+1}\frac{\partial\overline{\delta}(\overline{s},t)}{\partial\overline{s}}\frac{d\overline{s}}{\overline{x}-\overline{s}} \\ \implies I(x_i) &= \sum_{j=1}^{n}\frac{\pi}{n+1}(1-{s_j}^2)\frac{1}{x_i - s_j}\phi_j \\ \implies I(x_i) &= W_{ij}K_{ij}\phi_j \end{aligned} \tag{16}$$

$$F_i = (1-\frac{\tau_b}{f\sigma_0}) - \frac{\Delta p_{max} erfc\left(|\lambda x_i|\right)}{\sigma_0} + \frac{1}{2\pi}W_{ij}K_{ij}\phi_j \tag{17}$$

$$\begin{aligned} m_{n+1} &= m_n - J_n^{-1}m_0 \\ \implies dm &= -J_n^{-1}m_0 \end{aligned} \tag{18}$$

$$\begin{aligned} J_{1\ldots(n+1),1\ldots n} &= \frac{\partial F_i}{\partial\phi_j} = \frac{1}{2\pi}W_{ij}K_{ij}\phi_j \\ J_{1\ldots(n+1),n+1} &= \frac{\partial F_i}{\partial\lambda} = \frac{2}{\sqrt{\pi}}\exp -(\lambda x_i)\mid x_i\mid \end{aligned} \tag{19}$$

2. Rupture model for enhanced permeability pressure case

$$\tau_s(x,t) = f(\sigma_0 - \Delta p(x,t)) \tag{20}$$

where $\Delta p(x,t) = A_p(x)$

$$\tau_s(x,t) = \tau_b - \frac{\mu^*}{2\pi}\int_{a_-}^{a_+} \frac{\partial\delta(s,t)}{\partial s}\frac{ds}{x-s} \tag{21}$$

$$\begin{aligned} f(\sigma_0 - \Delta p(x,t)) &= \tau_b - \frac{\mu^*}{2\pi}\int_{a_-}^{a_+} \frac{\partial\delta(s,t)}{\partial s}\frac{ds}{x-s} \\ f(\sigma_0 - A_p(x)) &= \tau_b - \frac{\mu^*}{2\pi}\int_{a_-}^{a_+} \frac{\partial\delta(s,t)}{\partial s}\frac{ds}{x-s} \end{aligned} \tag{22}$$

$$(1 - \frac{\tau_b}{f\sigma_0}) - \frac{A_p(x)}{\sigma_o} = -\frac{1}{2\pi}\int_{-1}^{+1} \frac{\partial\bar{\delta}(\bar{s},t)}{\partial\bar{s}}\frac{d\bar{s}}{\bar{x}-\bar{s}} \tag{23}$$

$$\begin{aligned} I(x_i) &= \int_{-1}^{+1} \frac{\partial\bar{\delta}(\bar{s},t)}{\partial\bar{s}}\frac{d\bar{s}}{\bar{x}-\bar{s}} \\ \implies I(x_i) &= \sum_{j=1}^{n} \frac{\pi}{n+1}(1-{s_j}^2)\frac{1}{x_i - s_j}\phi_j \\ \implies I(x_i) &= W_{ij}K_{ij}\phi_j \end{aligned} \tag{24}$$

$$F_i = (1 - \frac{\tau_b}{f\sigma_0}) - \frac{A_p(x)}{\sigma_0} + \frac{1}{2\pi}W_{ij}K_{ij}\phi_j \tag{25}$$

$$\begin{aligned} m_{n+1} &= m_n - J_n^{-1}m_0 \\ \implies dm &= -J_n^{-1}m_0 \end{aligned} \tag{26}$$

$$\begin{aligned} J_{1\ldots(n+1),1\ldots n} &= \frac{\partial F_i}{\partial\phi_j} = \frac{1}{2\pi}W_{ij}K_{ij}\phi_j \\ J_{1\ldots(n+1),n+1} &= \frac{\partial F_i}{\partial a(t)} = \frac{\partial}{\partial a(t)}A_p(x) \\ &= \frac{\partial}{\partial x}A_p(x)\frac{\partial x}{\partial\bar{x}}\frac{\partial\bar{x}}{\partial a(t)} \\ &= \frac{\partial}{\partial x}A_p\frac{x}{a} = \frac{\partial}{\partial x}A_p\bar{x} \end{aligned} \tag{27}$$

3. Approximation schema for pressure gradient, from the supplied pressure vector and subsequent interpolation

$$\left.\frac{dA_p(x)}{dx}\right|_i = \frac{-3A_i + 4A_{i+1} - A_{i-1}}{2\Delta x} \tag{28}$$

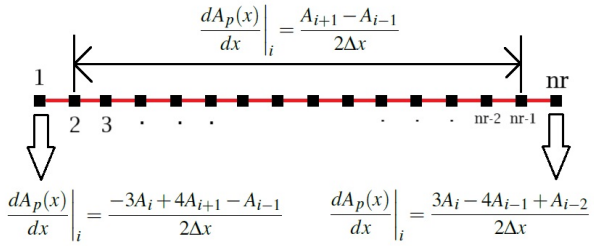

$$\left.\frac{dA_p(x)}{dx}\right|_i = \frac{3A_i - 4A_{i-1} + A_{i-2}}{2\Delta x} \tag{29}$$

$$\left.\frac{dA_p(x)}{dx}\right|_i = \frac{A_{i+1} - A_{i-1}}{2\Delta x} \tag{30}$$

IV. RESULTS

A. Solution for a first-order ODE

The algorithm performs well in this case. It responds to the problem by shortening the step size at the inflection point. It also gradually expands the step size as the curve moves away from the inflection point in the graph of the function. At the end, it is seen that the step size contracts to meet the limit of $t = 10$ that has been set in the parameters for the code.

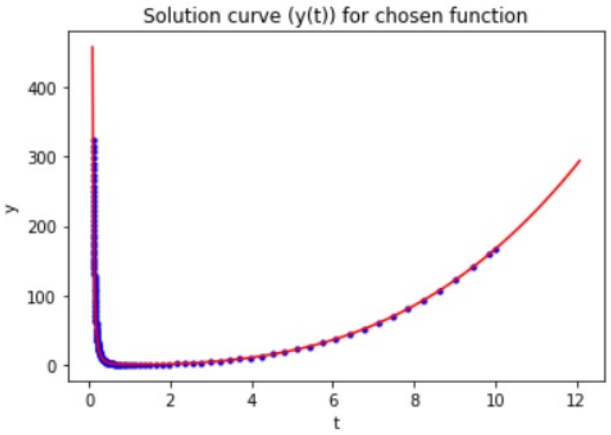

FIG. 1. Solution in Scenario 1 using RKF45

B. Earth Hole problem

It was seen that the computed solution is highly accurate as compared to the analytical solution. The modification made to the code successfully allows for the prevention of the division by zero error when Δ is to be

calculated. We also successfully verify the solution to the problem that we obtained while obtaining the analytical solution - it takes almost 5063 seconds for the body dropped from one end of the Earth to return to the same end again. The order of error is seen to be less than 1 part in 10^5 if the position of the body at $t = 5063$s is checked.

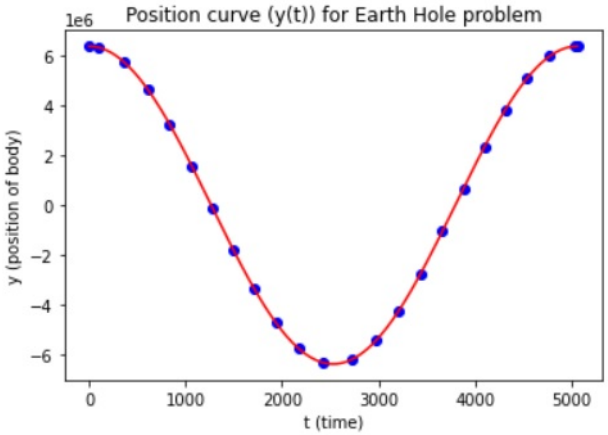

FIG. 2. Solution in Scenario 2 using RKF45

Again, we observe that the step size changes marginally to become smaller when reaching the other side of the Earth, since the position curve experiences an inflection point during that time. It remains large when the body is moving the fastest (near the centre of the Earth).

C. Predator-Prey system

Similar to [1], the birth rate (a) and death rate (c) parameters were varied and the results were recorded for various cases. It was seen that the maximum populations of the prey and predator species increased dramatically with each "period", as opposed to a much slower increase. It is difficult to tell if this is a more accurate or a less accurate solution that the one provided in Juarlin's paper, since no analytical solution exists for this system of equations. However, we can clearly see how the step size changes multiple times during a single period to accommodate for both the prey and predator solution curves. In all the cases seen below, t was initialised at $t = 0$ and terminated at $t = 500$, taking an execution time of about a second.

First (Figure 3), we set a, c, α, γ, $x(t = 0)$, and $y(t = 0)$ as 0.1 to get a base case with which to compare our other results, as was done in [**?**]. Here, we see the same sort of oscillatory behaviour as seen in [**?**], but with a key difference - the maximum population and the period of oscillation keep increasing as time progresses.

Next (Figure 4), we set a as 0.3 and c as 0.2. We can see that this results in a much smaller period for the oscillation of the population curves, as the prey species is

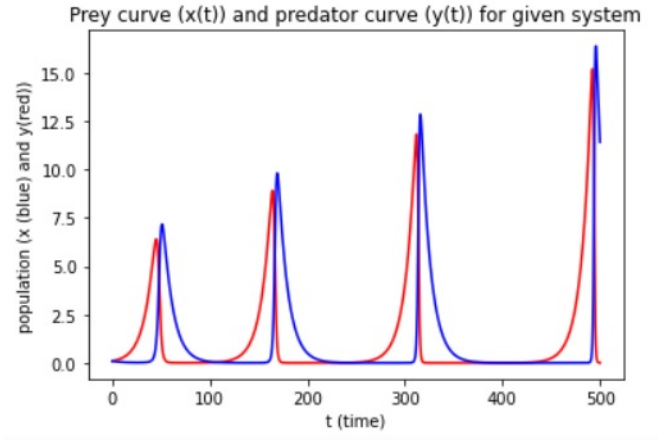

FIG. 3. Scenario 3 with $a = 0.1$ and $c = 0.1$

produced much quicker while the predator is also eliminated quicker (leading the prey species to proliferate).

Finally (Figure 5), we look at a system where the predators die rapidly ($c = 0.3$) while the prey species are born at the same rate as the first case ($a = 0.1$). We see that a large amount of prey animals are needed before the predator population rises significantly.

It is ultimately difficult to comment on the accuracy of these results, as not much literature exists on this particular application of the RKF45 algorithm.

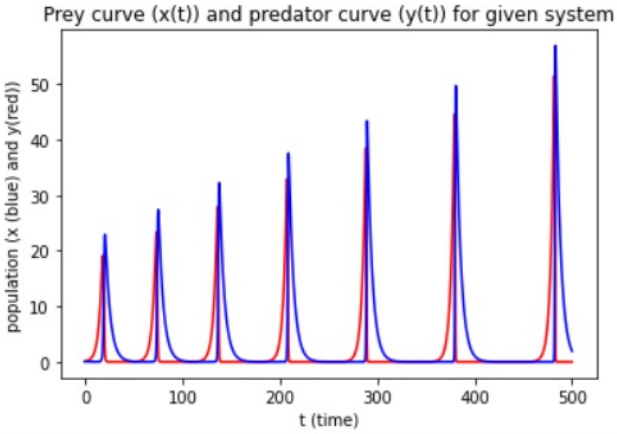

FIG. 4. Scenario 3 with $a = 0.3$ and $c = 0.2$

V. CONCLUSION

We hence come to the conclusion that the aseismic slip front is seen to outpace the pore pressure front in particular cases of low stress drops on the fault in case of fluid injection, when we take permeability enhancement into account. Thus, this can help to explain the anomalously high hydraulic diffusivities seen in case of in-situ observations when compared to laboratory measurements for core samples.

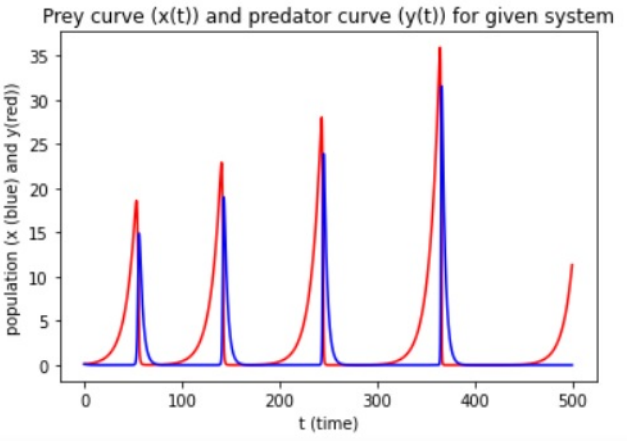

FIG. 5. Scenario 3 with $a = 0.1$ and $c = 0.3$

ACKNOWLEDGMENTS

I would like to convey my thanks to Dr Subhashis Basak and Dr Pathikrit Bhattacharya for giving me the opportunity to work on this project. This project gave me my first opportunity to learn about finite element methods. This gave me the know-how to use them to solve problems in continuum mechanics, rock mechanics, and fracture mechanics.

[1] Bhattacharya, P. and Viesca, R. C. (2019). Fluid-induced aseismic fault slip outpaces pore-fluid migration. *Science*, 364(6439):464–468. Publisher: American Association for the Advancement of Science.

[2] Keranen, K. M., Weingarten, M., Abers, G. A., Bekins, B. A., and Ge, S. (2014). Sharp increase in central oklahoma seismicity since 2008 induced by massive wastewater injection. *Science*, 345(6195):448–451.